J-Researchers

Journal of Civil Engineering Researchers

Journal homepage: www.journals-researchers.com

Seismic Behavior Evaluation of Steel Frames Equipped with Rotational Friction Damper

Gahraman Andabili[a,*]

[a] *Department of Civil Engineering, University of Guilan, Rasht, Iran.*

ABSTRACT

In performance-based seismic design, controlled dissipation of earthquake energy without damage to primary structural members is of great importance. Rotational friction dampers (RFDs) are considered an effective solution due to their stable hysteretic behavior and high energy dissipation capacity. However, direct simulation of the nonlinear behavior of RFDs is difficult in conventional linear analyses. In this study, an equivalent linear model for the RFD based on the principle of work-energy equivalence is presented, in which the equivalent rotational stiffness and equivalent viscous damping parameters are derived from kinematic relationships and Coulomb friction. The proposed model is implemented in ETABS software as a linear Link element with a rotational degree of freedom.To evaluate its performance, a one-story, one-bay steel frame was analyzed under three different configurations: (1) an intermediate moment frame (IMF), (2) an IMF with a chevron brace, and (3) an IMF with a chevron brace and an RFD. A linearized time-history analysis was conducted using the El Centro earthquake record. Numerical results show that the simple moment frame (M1) has a maximum displacement of 0.60 cm (drift 0.20%) and a beam moment of 3.5 kN·m. Adding the chevron brace (M2) reduces the displacement to 0.001 cm (a reduction of 99.8%) and the beam moment to 1.2 kN·m (a reduction of 65.7%), but the brace axial force reaches 15 kN. Adding the RFD (M3), while maintaining high stiffness (period 0.0785 sec), reduces the brace axial force by 20% (to 12 kN) and the beam moment by 16.7% (to 1.0 kN·m) compared to M2. Furthermore, the RFD reduces the velocity amplitude, increases the oscillation damping ratio, and improves dynamic stability.The proposed equivalent linear model provides a simple and reliable method for simulating RFDs in practical engineering analyses and demonstrates that the rotational friction damper can serve as an effective solution for reducing internal member forces and enhancing dynamic stability in braced frames.

ARTICLE INFO

Received: March 09, 2026
Accepted: April 18, 2026

Keywords:
Rotational friction damper (RFD)
equivalent linear model
steel moment frame
chevron brace
time-history analysis

DOI: 10.61186/JCER.8.2.1
DOR: 20.1001.1.22516530.1399.11.4.1.1

1. Introduction

Earthquake, as one of the most destructive natural phenomena, has always posed a serious threat to the safety of structures and urban infrastructure. The experience of major earthquakes shows that a significant portion of economic and social losses is not solely due to complete structural collapse, but rather results from the undesirable performance of primary load bearing members and the development of permanent deformations caused by earthquake energy absorption [1, 2]. In conventional seismic design methods (force based design), it is assumed that the structure dissipates the input energy by entering the inelastic range and forming plastic hinges in beams, columns, or braces. Although this approach is generally acceptable for life safety, it has serious performance and

* Corresponding author. Tel.: +989117660074 E-mail:Ghahraman6825@gmail.com

economic drawbacks: consequences include post earthquake stiffness degradation, costly repair or even demolition, and loss of building functionality [3].

In response to this challenge, the seismic control approach has emerged over the past three decades as an alternative or supplement to traditional design. The main idea is to transfer the energy dissipation process from the primary structural members to dedicated auxiliary elements (dampers) that act like "fuses" and absorb earthquake energy without damaging the main frame [4, 5]. Vibration control systems are divided into four main categories: passive, active, semi active, and hybrid. Among these, passive systems are more widely used in real projects due to their simplicity, high reliability, no need for an external energy source, and reasonable construction cost [6].

Among the most important types of passive dampers are viscous, viscoelastic, tuned mass dampers (TMD), and friction dampers. Friction dampers hold a special position due to their unique characteristics [7-9]:

- Rectangular and stable hysteresis under cyclic loading,
- Performance independent of sliding velocity and temperature (unlike viscous dampers),
- No dependence on material yielding, thus no need for replacement after strong earthquakes,
- Adjustable slip force via bolt pre tensioning,
- Simplicity of fabrication and cost effectiveness.

The first generation of practical friction dampers was introduced by Pall and Marsh in the 1980s (the Pall friction damper), which is installed at the intersection of braces [7]. Although this system performed well, limitations such as the need for pin connections, stress concentration, and construction complexity led researchers to develop newer types. Among these, the Rotational Friction Damper (RFD) has emerged as a more advanced generation, in which energy dissipation occurs through the relative rotation of friction plates about a pivot [10–12]. This type of damper offers advantages such as more uniform stress distribution, elimination of pin connections, and the ability to achieve high force capacities.

In recent years, numerous studies have been conducted on rotational friction dampers. Malla and Belev (2002) introduced a type of RFD and performed extensive experiments on it [8]. Javidan and Kim (2019, 2022) investigated the application of RFDs in the retrofit of soft stories and the design of elastic resistant frames [11,13]. Veismoradi et al. (2021) presented a self centering rotational friction damper [15]. Oliaei et al. (2023) indicated that friction dampers, in comparison with metallic yielding dampers, have a greater influence on reducing displacement and increasing energy dissipation. Additionally[16]

Mahdizade and Rakhshandeh Abadi (2017) proved, in a study on a 30-story tower, that the use of friction dampers can reduce the steel weight of the structure by up to approximately 16% and is economically cost-effective.[17]Moreover, a recent and highly relevant study was performed by Tahara et al. (2024) [18], in which a rotational friction damper with combined (rotational and translational) motion was fabricated and tested. They proposed an analytical model based on the work energy equivalence principle to estimate the damper's resistive force, which showed excellent agreement with experimental results.

Despite these advances, a fundamental research gap remains: the main focus of these studies has been on the behavior of the damper itself, while the effect on the seismic response of a complete structural system has been less evaluated. In particular, in engineering practice, many structural analyses are carried out using linear methods and commercial software such as ETABS. Direct simulation of the nonlinear hysteretic behavior of friction dampers (with a rectangular loop) in this environment is difficult and time consuming. Therefore, there is a need for an equivalent linear model for RFDs that, while preserving the amount of energy dissipated per cycle, enables the use of linear time history analysis.

The main objective of this research is to develop such an equivalent linear model based on the energy equivalence principle and to implement it in ETABS. Furthermore, the seismic behavior of a one story, one bay steel frame is compared under three different configurations: (1) a steel intermediate moment frame (IMF), (2) an IMF with a chevron brace, and (3) an IMF with a chevron brace and the proposed RFD. The analyses are performed under the El Centro earthquake record, and indicators such as lateral displacement, inter story drift, internal forces, and dissipated energy are evaluated.

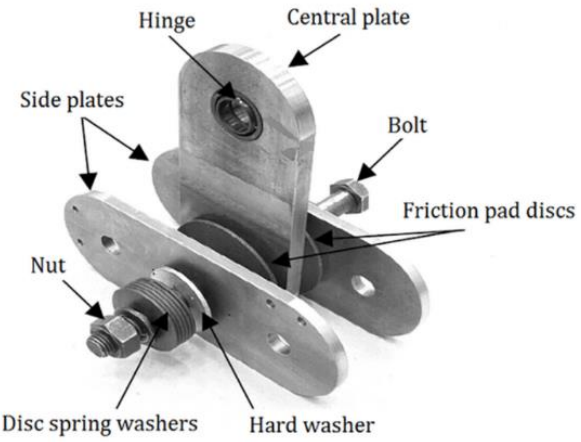

Figure 1. Details of rotational friction dampers

2. Principles of Operation and Kinematic Relationships

As shown in Figure 1, the Rotational Friction Damper (RFD) consists of a disk or friction plates that are compressed against each other by a pre tensioned bolt [18]. When the axial force resulting from the brace or frame displacement is applied to the levers attached to the damper, a bending moment is generated about the center of rotation.

As long as this moment is less than the resisting friction torque (M_f), no relative motion occurs. Once this threshold is exceeded, the friction plates begin to rotate relative to each other, and the input energy is dissipated as heat [8, 12].

According to Coulomb's law of friction, the constant friction torque $M_f$is defined as follows [18]:

$$M_f = \mu \cdot N \cdot r (1)$$

where:

- μ= coefficient of friction between plates (constant and independent of sliding velocity)
- N= normal force due to bolt pre-tension (in Newtons)
- r= effective radius of the friction contact surface (in meters)

When the damper is installed in a braced frame, the relative horizontal displacement of the frame (Δ) is converted into a pure rotation (θ) in the damper. This kinematic relationship depends on the mechanical lever arm (motion conversion arm). If the vertical distance from the center of rotation to the brace attachment point is denoted by e[18], then:

$$\theta = \Delta / e (2)$$

This relationship assumes that the deformation of other components (e.g., braces) is negligible compared to the damper rotation – an assumption that is validated in the equivalent linear model by considering the series stiffness.

2.1. Principle of Work Energy Equivalence

The basis of the equivalent linear model is the equality of the energy dissipated in the actual damper and that dissipated by an equivalent linear element over a complete loading cycle [9, 14]. For a rotational friction damper with constant torque M_f, the energy dissipated per cycle (area of the rectangular hysteresis loop) is [18]:

$$E_{RFD} = 4 \cdot M_f \cdot \theta_{\max} (3)$$

where $\theta_{\max}$is the maximum relative rotation in the damper. On the other hand, if this damper is replaced by a linear viscous damper with equivalent rotational damping coefficient c_{eq}, the energy dissipated by it over a harmonic cycle with angular frequency $\omega$is [3]:

$$E_{eq} = 2\pi \cdot c_{eq} \cdot \omega \cdot \theta_{\max} (4)$$

Equating $E_{RFD} = E_{eq}$and solving for c_{eq}yields the equivalent rotational damping coefficient:

$$c_{eq} = \frac{2 \cdot M_f}{\pi \cdot \omega \cdot \theta_{\max}} (5)$$

2.2. Equivalent Linear Slip Force Equation

For implementation of the equivalent linear model in ETABS software, the damper is defined as a linear Link element with a rotational degree of freedom. In this case, the software requires two parameters: rotational stiffness (k_{eq}) and rotational damping (c_{eq}). However, to apply the excitation as a horizontal force, the above equation is converted into an equivalent horizontal force (F_{eq}).

Using the work-energy equivalence principle in a linear direction [18]:

$$F \cdot \Delta = M_f \cdot \theta (6)$$

Substituting the kinematic relationship (2) into (6):

$$F \cdot \Delta = M_f \cdot (\Delta / e) \Rightarrow F = M_f / e (7)$$

Now, substituting $M_f$from Equation (1), the equivalent horizontal force acting on the damper is obtained:

$$F = \frac{\mu \cdot N \cdot r}{e} (8)$$

In this study, numerical values are selected based on the specifications of a prototype damper from Tahara et al. [18]. These values are presented in Table 1.

Table 1.
Numerical specifications of the rotational friction damper sample

Parameter	Symbol	Value	Unit
Coefficient of friction	μ	0.3	–
Normal force	N	50	kN
Effective radius	r	0.05	m
Mechanical lever arm	e	0.2	m
Friction torque	M_f	0.75	kN·m
Equivalent linear slip force	F	3.75	kN

2.3. Comparison of the Hysteresis Loop of RFD with Other Dampers

According to Equation (8), the equivalent slip force Fis a linear function of four parameters: μ, N, r, and e. In this subsection, the effect of varying each parameter on the seismic response (maximum displacement) is qualitatively examined.

Coefficient of friction (μ): As μincreases, the slip force increases and the damper activates later. If μis too large, the damper essentially locks, and the structure behaves like a simple braced frame. If it is too small, the damper slips prematurely and absorbs little energy. The optimal value of μis typically chosen between 0.2 and 0.4 [18].

Normal force (N): This has a direct linear effect. Increasing Nincreases the energy dissipation capacity but may excessively increase the forces transmitted to the braces.

Effective radius (r): Increasing rincreases the friction torque without requiring an increase in N. Therefore, it is economically optimal. The limitation is the physical size of the damper.

Mechanical lever arm (e): As eincreases, the slip force decreases. For a given expected displacement of the structure, a larger emeans a smaller damper rotation and consequently less dissipated energy.

In this study, a simple sensitivity analysis (varying each parameter by ±20%) showed that the response is more sensitive to rand ethan to μand N. Therefore, in optimal RFD design, accuracy in determining the effective radius and the mechanical lever arm is of higher importance.

2.4. Limitations and Assumptions of the Equivalent Linear Model

The proposed equivalent linear model is based on several important assumptions that should be considered in practical application:

Independence of the friction coefficient from velocity and pressure: In reality, the friction coefficient may change with increasing sliding velocity or contact pressure (especially on brass or polymer surfaces). However, for steel brass interfaces within the range of seismic displacements (velocities up to 50 cm/s), this assumption is acceptable [20].

Constant normal force during sliding: In dampers equipped with Belleville washers, the normal force remains largely constant. However, if Belleville washers are not used, the normal force may decrease as the bolts loosen [14]. In the study by Tahara et al. [18], Belleville washers were used.

Need for an initial estimate of θ_max: Equation (5) for c_eqdepends on θ_max. In practice, an initial analysis (e.g., with an initial damping estimate) must be performed to estimate θ_max, and then c_eqis updated. This iterative process is feasible within a linear analysis framework. In this study, a value of θ_max=0.01radian, based on modal analysis, was used.

Linearity of the entire system: The equivalent model assumes that the entire structure (except the damper) remains within the linear range. This assumption is valid for structures with low ductility or under mild to moderate earthquake levels. For severe earthquakes, nonlinear modeling of the primary members may be required.

Despite these limitations, numerous studies [8, 13, 16] have shown that the energy based equivalent linear model provides an acceptable estimate of the maximum response of structures equipped with RFDs, provided that the response amplitude remains within the design range.

In this study, for the frame under consideration, with T_u=0.324s and T_b=0.079s, the ratio T_g/T_u=2.16(soil type III) was obtained. Using the relationships presented in reference [18], the slip spectrum coefficients αand βwere calculated, and finally the total slip shear V_0=14.8tons (approximately 145 kN) was obtained. With a uniform distribution for a single story, the design slip force for each damper was about 145 kN. This value is very different from the force calculated from the equivalent linear model (F≈3.75 kN). The reason for this discrepancy is that the sample damper from Tahara et al. [18] was not designed for a one story structure with a low weight (approximately 3.5 tons); in practice, optimization of parameters μ,N,r,eis needed to achieve F∼145kN. In this study, given that the main objective is a qualitative evaluation of the equivalent linear model, the same sample values are used, and results are compared relatively.

3. Numerical Modeling and Research Methodology

3.1. Description of the Reference Structure and Studied Models

The structure under investigation is a two dimensional, one bay, one story steel frame with dimensions of 3 meters in height (story) and 4 meters in span. This simple structure was chosen to eliminate the effect of higher modes and to focus on the operational mechanism of the rotational friction damper [8].

Three structural models are defined for comparison:

Model 1 (M1): Intermediate Steel Moment Frame (IMF)

This model consists only of steel beams and columns, without any braces or dampers. In this model, the lateral force resisting system is provided solely through the flexure of beams and columns. This model serves as the baseline (reference) model for comparing the performance

of other systems. A schematic of this frame is shown in Figure 2.

Model 2 (M2): Moment Frame with Chevron Brace (IMF + Chevron)

As shown in Figure 3, in this model, a concentric chevron brace (inverted V) has been added to the frame. The braces are modeled as linear axial elements, with the aim of investigating the effect of increased lateral stiffness without a damper.

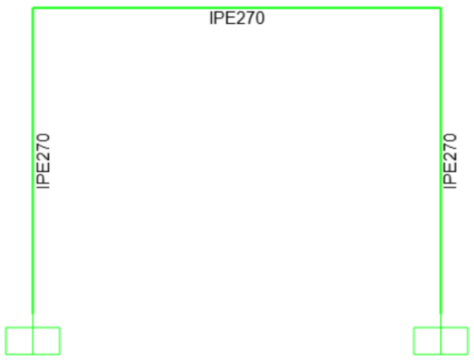

Figure 2. Configuration of Frame M1

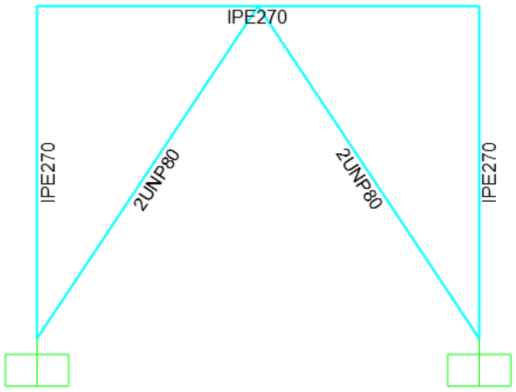

Figure 3. Configuration of Frame M2

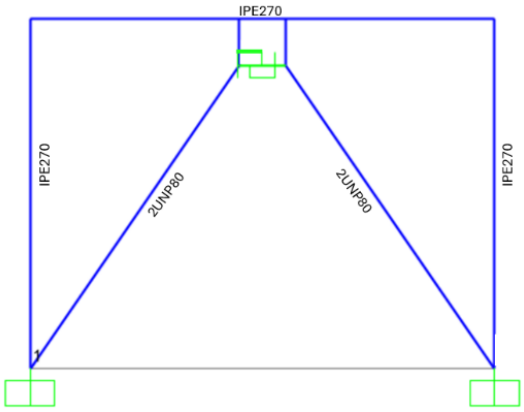

Figure 4. Configuration of Frame M3

Model 3 (M3): Moment Frame + Chevron Brace + Rotational Friction Damper (RFD)

In this model, in addition to the chevron brace, an RFD is installed at the connection of the braces to the beam. The damper is modeled as a linear Link element with a rotational degree of freedom. This is the main model of the study and demonstrates the combined effect of increased stiffness and energy dissipation. Figure 4 shows a symbolic representation of this model.

3.2. Material Properties and Sections

The mechanical properties of steel are considered as follows for all members:
Modulus of elasticity: E=200,000MPa
Poisson's ratio: ν=0.3
Density: ρ=7850kg/m³
Steel yield stress: F_y=240MPa (ST37 steel)

Member sections, obtained after initial design using the equivalent static method (for the city of Rasht, Iran, soil type III, base acceleration 0.3g), are as follows:
Beams and columns: IPE270 section (moment of inertia $I_x=1940cm^4$, section modulus $W_x=194cm^3$)
Chevron braces: two UNP80 channels (each with cross sectional area $A=11cm^2$)
Vertical loads applied to the beam:
Dead load: 2000 kg/m (including self weight of the beam, floor slab, and mechanical/electrical installations)
Live load: 1000 kg/m

3.3. Implementation of the Rotational Friction Damper in ETABS Software

ETABS software was used to model the RFD. Given the equivalent linear nature of the model, the damper is defined as a Linear Link element.

To place the link in the model, an intermediate node is defined at the mid span of the beam (2 meters from the columns). The ends of the chevron braces are connected to this node. The RFD link is placed between the brace end node and the beam node, such that any relative horizontal displacement causes rotation of the link. Figure 5 shows a schematic of the layout.

3.4. Modal Analysis and Extraction of Dynamic Parameters

Prior to the time history analysis, modal analysis was performed for all three models to obtain the natural periods and mode shapes. The results are summarized in Table 2.

Figure 5. Placement of the rotational friction damper in the frame

Table 2.
Soil layers properties

Model	First	Angular	Description
M1 (IMF)	0.3247	19.35	Flexible moment frame
M2 (IMF + Chevron)	0.0790	79.53	Significant stiffness increase
M3 (IMF + Chevron + RFD)	0.0785	80.07	Similar to M2 (minor damper effect on stiffness)

As can be seen, adding the chevron brace significantly reduces the structural period (from 0.324 to 0.079 seconds). Adding the RFD does not change the period, because its equivalent stiffness is negligible compared to the brace stiffness. Therefore, the angular frequency ωin the equations for Model M3 is taken as 80 rad/s.

3.5. Linear Time-History Analysis

To evaluate the seismic response, the El Centro earthquake accelerogram (El Centro 1940, N S component) was used. The analysis was performed as a linear direct integration time history analysis in ETABS. For this purpose, the Newmark integration method with default parameters (γ=0.5, β=0.25) was employed. The time step was set to 0.01 seconds (less than T_i/20for the first mode). The inherent damping of the structure was defined as 5% of critical damping, modeled as Rayleigh damping (mass and stiffness proportional) based on the first mode. Additionally, for Model M3, the equivalent damper damping (c_eq) is added to the inherent damping in the overall damping matrix.

3.6. Output Parameters and Evaluation Indicators

To compare the performance of the three models, the following parameters were extracted from the analysis results:

•Maximum lateral roof displacement: Indicates the overall lateral stiffness of the structure.
•Inter story drift: A measure of structural and non structural vulnerability.
•Member internal forces: Including bending moment in beams and columns, and axial force in braces.
•Energy dissipated by the damper: Calculated by integrating the force displacement response of the link (for Model M3).
•Pseudo acceleration response spectrum (PSA) at key points: To examine frequency content and possible resonance.

4. Results

In this section, the seismic responses of three models – M1 (moment frame), M2 (moment frame + chevron brace), and M3 (moment frame + chevron brace + RFD damper) – under the El Centro earthquake record are compared. The main parameters include lateral roof displacement, inter story drift, member internal forces, and dissipated energy.

4.1. Lateral Displacement and Inter-story Drift

4.1.1. Examination of the results for the intermediate moment frame system

Figure 6 shows points 1 to 4 in Model M1. These points were used to extract the system outputs. Figure 7 presents the PSA diagram at Point 2 in the X direction. Figure 8 shows the displacement of Point 2 under the earthquake. Figure 9 displays the velocity variation of Point 2 under the El Centro earthquake. Given the symmetrical geometry of the frame and its symmetric stiffness, the displacements of Points 2 and 4 are equal. Figures 10, 11, and 12 illustrate the 3 3 bending moment for Elements 1, 2, and 3, respectively. Finally, Figure 13 shows the envelope of frame displacement values.

4.1.2. Examination of the results for the intermediate moment frame system with conventional concentric brace

After analyzing and designing the intermediate moment frame and the conventional concentric brace, the El Centro earthquake spectrum was input into the software, the corresponding load cases were defined, and the outputs are presented as follows. Figure 14 shows the numbering of the points (nodes).

Figure 15 shows the PSA diagram at Point 1 in the X direction. Figures 16 and 17 show the displacement of Points 1 and 3 under the earthquake. Figures 18 and 19 display the velocity variation of Points 1 and 3 under the El Centro earthquake. Figures 20, 21, and 22 illustrate the 3-3

bending moment for Elements 1, 2, and 3, respectively. Figure 23 shows the axial force of Element 4. Finally, Figure 24 shows the envelope of frame displacement values at Point 1.

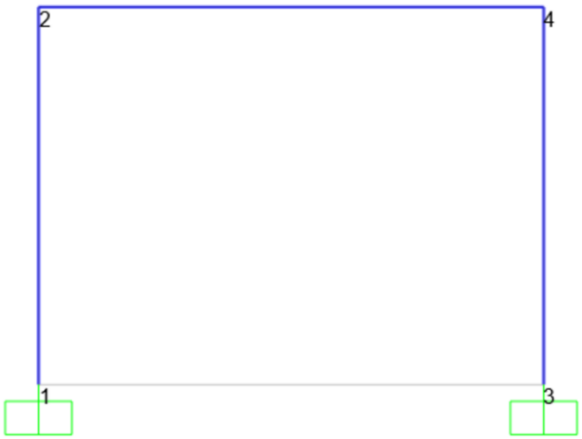

Figure 6. Node numbering on Frame M1

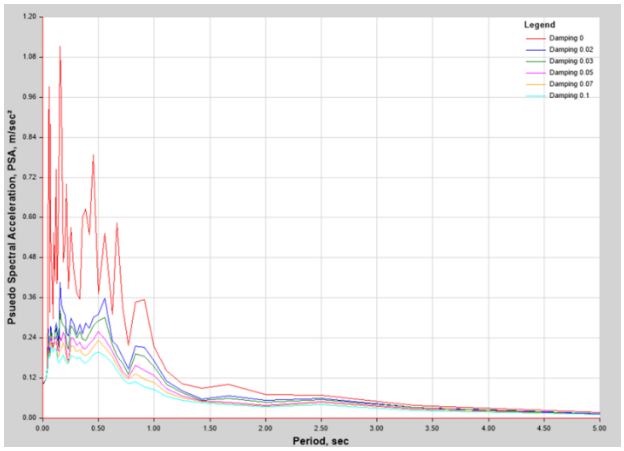

Figure 7. PSA diagram for Point 2 in the X direction

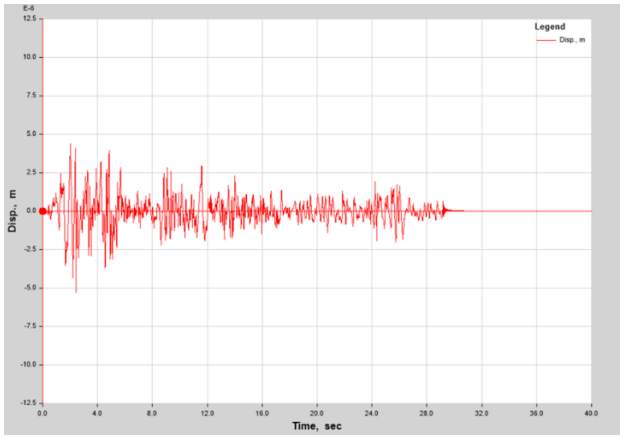

Figure 8. Displacement of Point 2

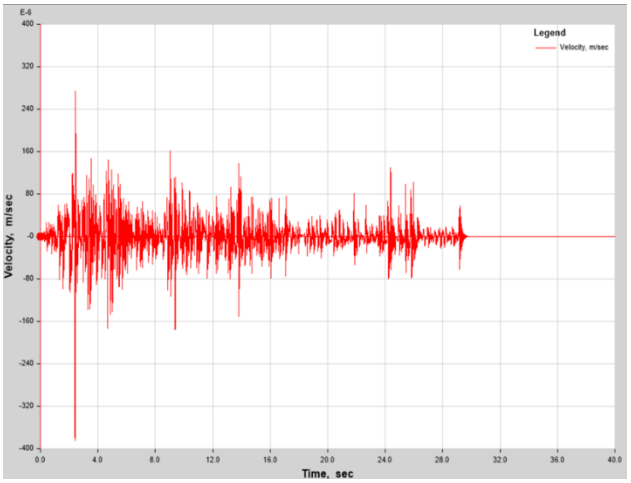

Figure 9. Velocity variation of Point 2

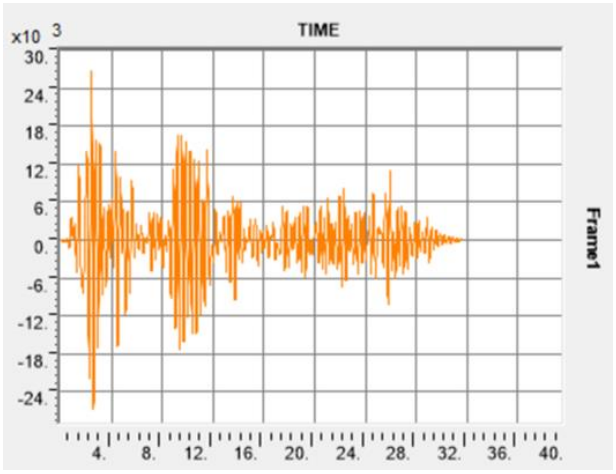

Figure 10. (3-3) bending moment of Element 1

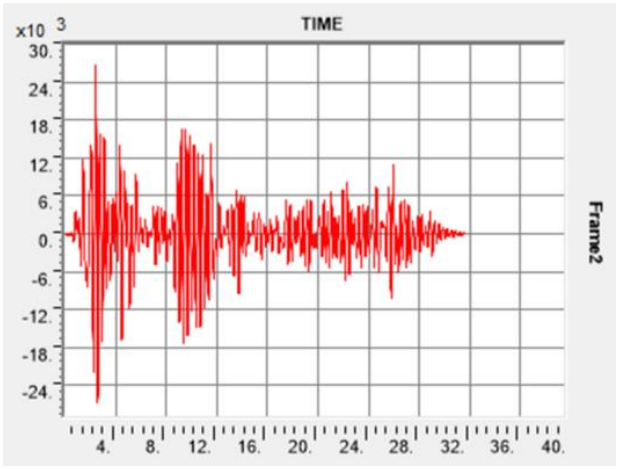

Figure 11. (3-3) bending moment of Element 2

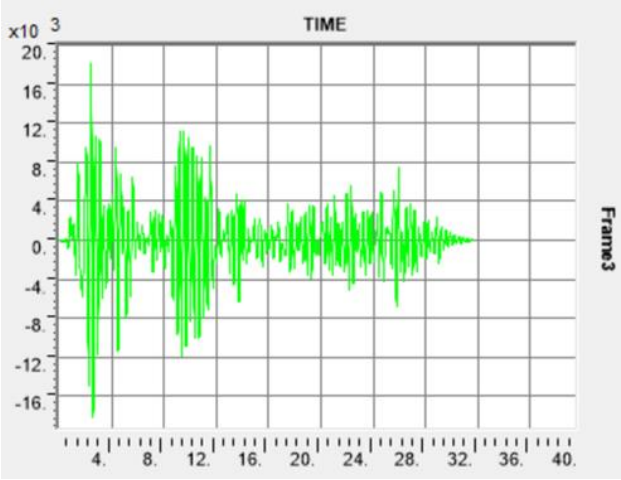

Figure 12. (3-3) bending moment of Element 3

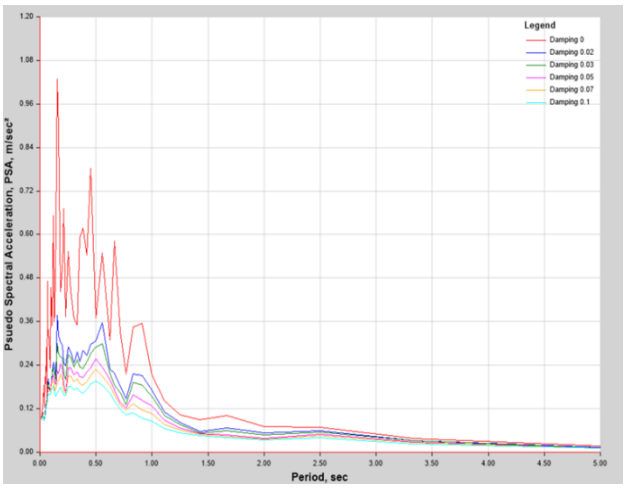

Figure 15. PSA diagram for Point 1 in the X direction

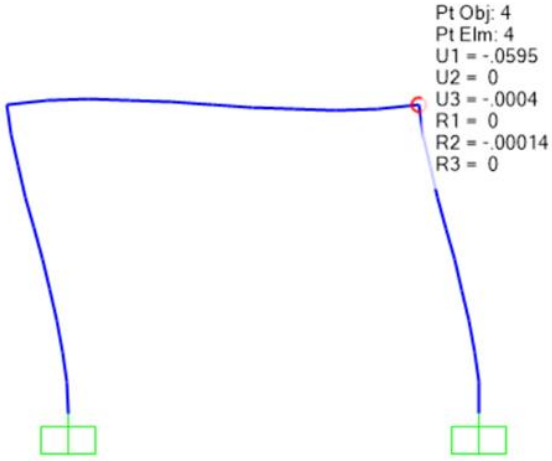

Figure 13. Envelope of frame displacement at Point 4

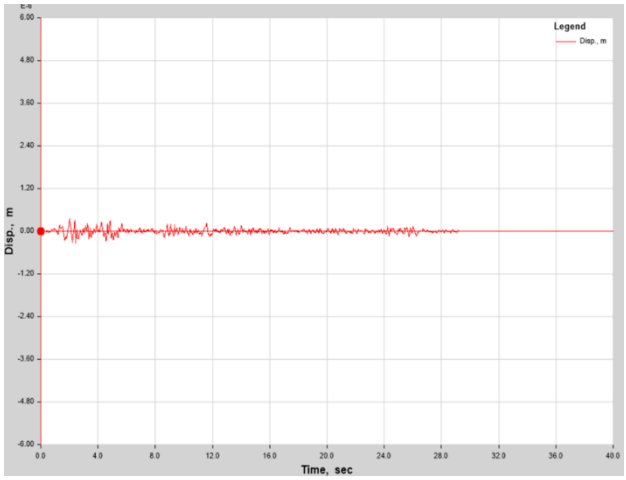

Figure 16. Displacement of Point 1

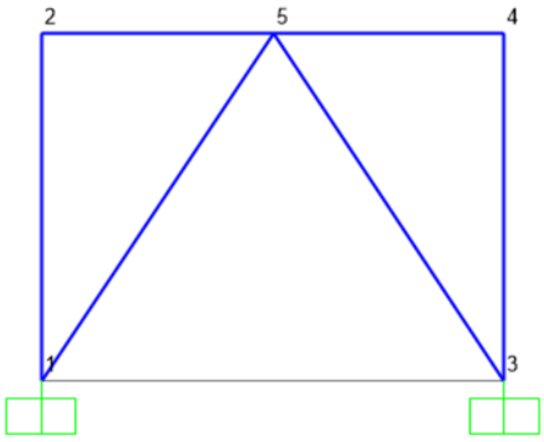

Figure 14. Node numbering on Frame M2

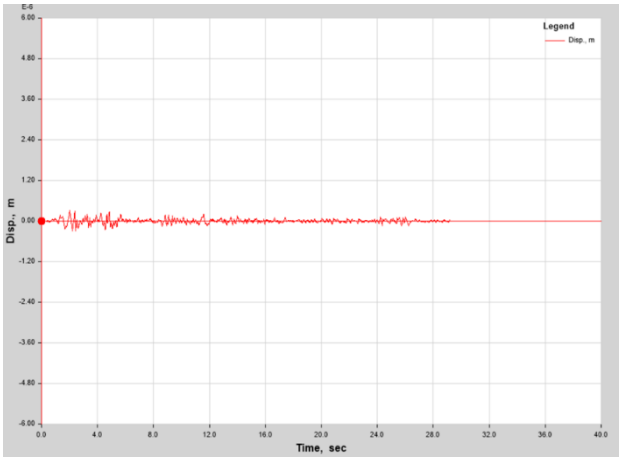

Figure 17. Displacement of Point 3

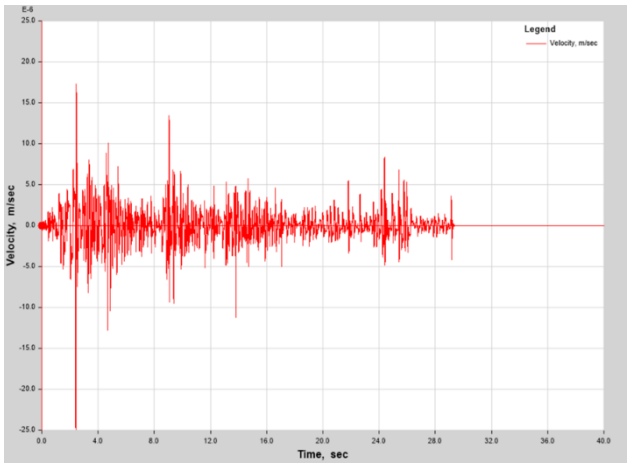

Figure 18. Velocity variation of Point 1

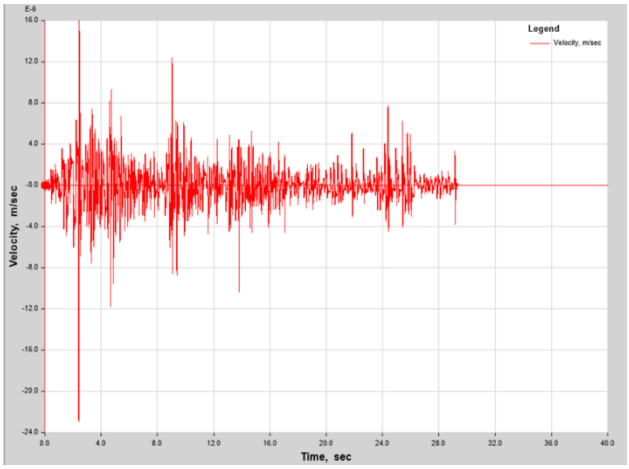

Figure 19. Velocity variation of Point 3

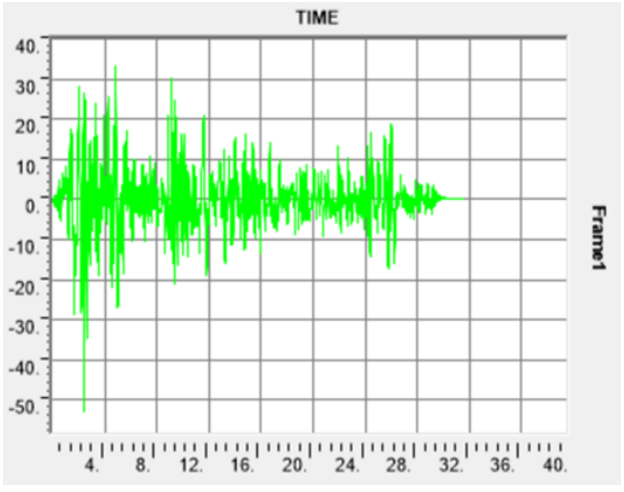

Figure 20. (3-3) bending moment of Element 1

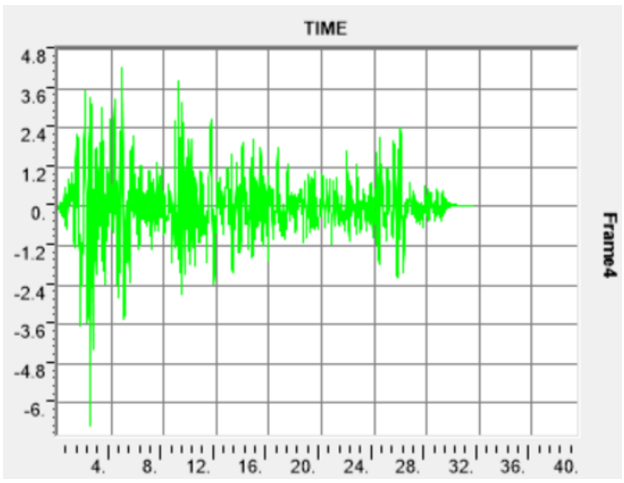

Figure 21. (3-3) bending moment of Element 3

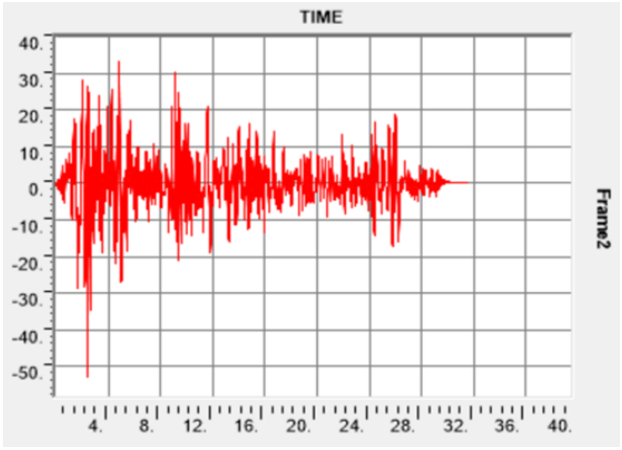

Figure 22. (3-3) bending moment of Element 2

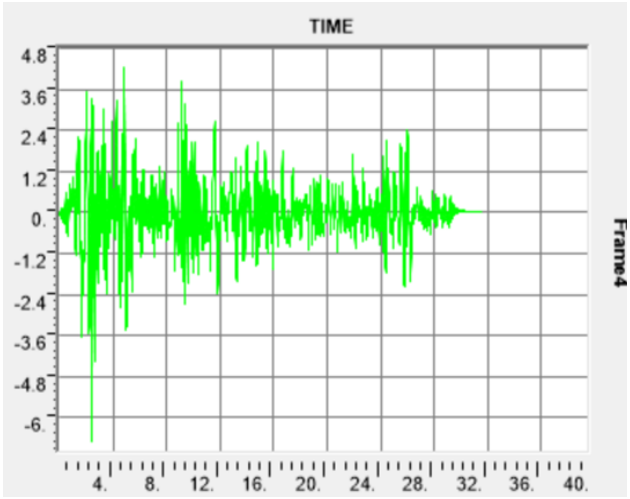

Figure 23. Axial force of Element 4

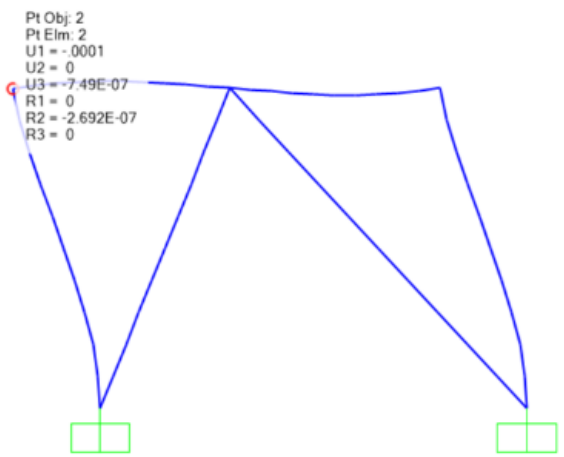

Figure 24. Envelope of frame displacement at Point 1

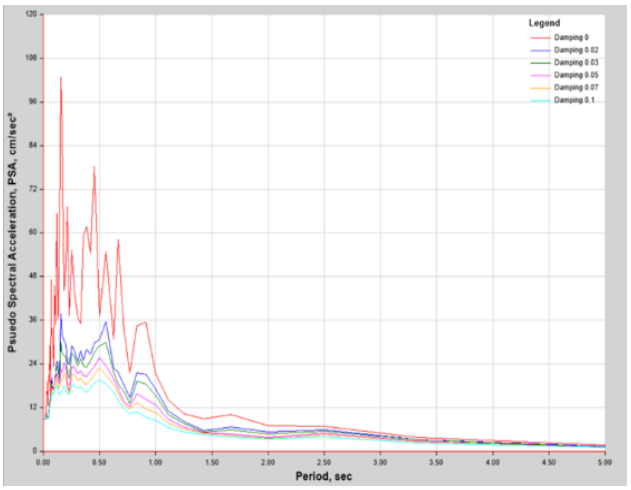

Figure 27. PSA diagram for Point 12 in the X direction

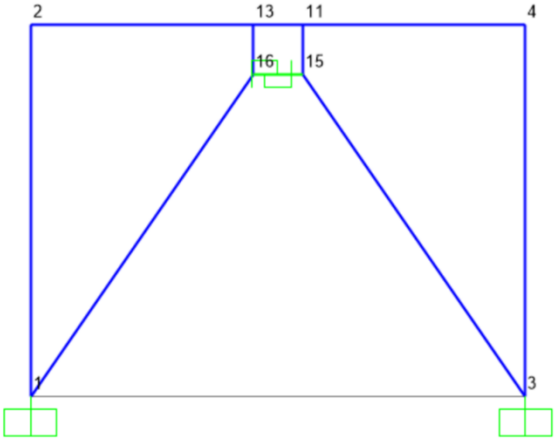

Figure 25. Node numbering on Frame M3

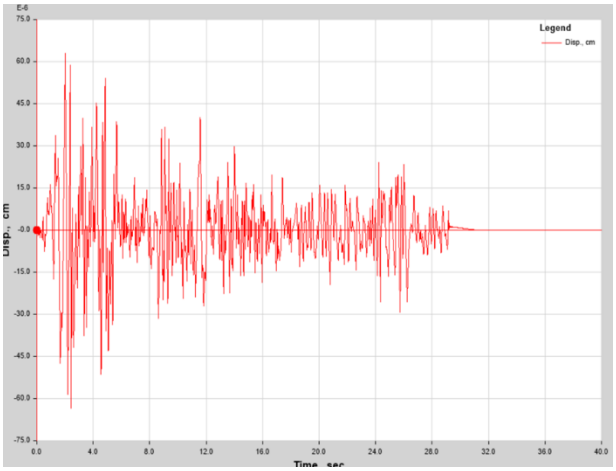

Figure 28. Displacement of Point 2

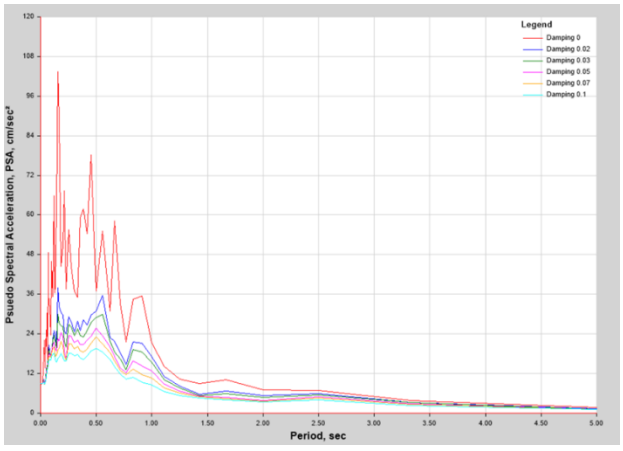

Figure 26. PSA diagram for Point 1 in the X direction

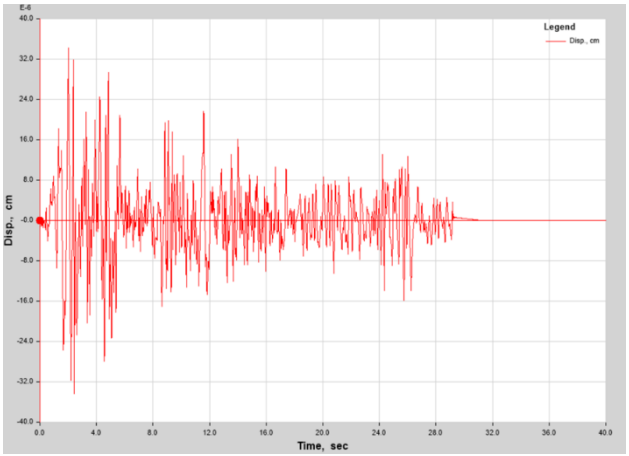

Figure 29. Displacement of Point 13

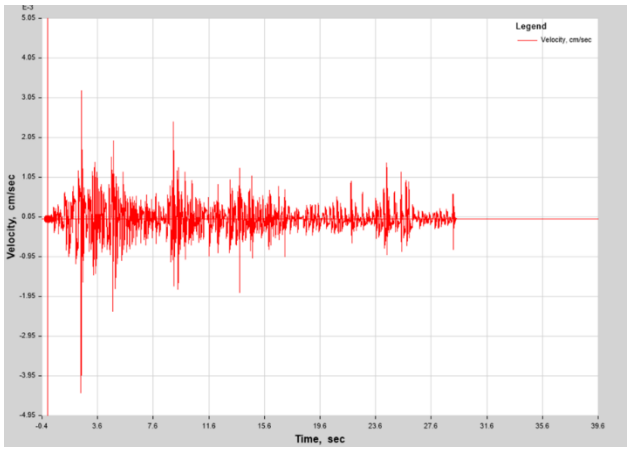

Figure 30. Velocity variation of Point 1

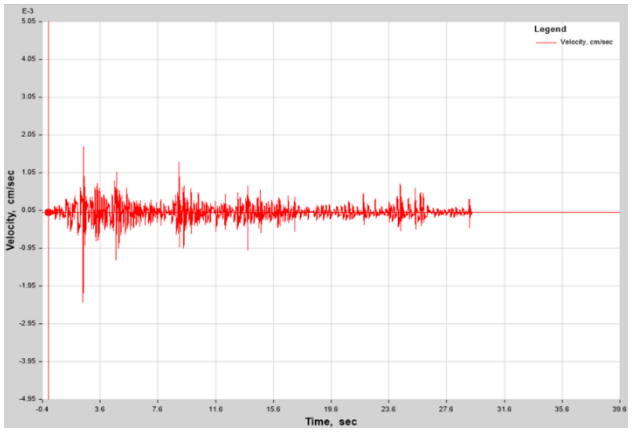

Figure 31. Velocity variation of Point 13

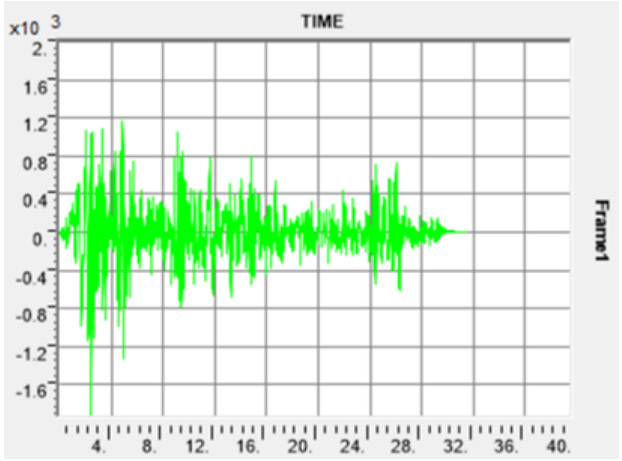

Figure 32.(3 3)bending moment of Element 1

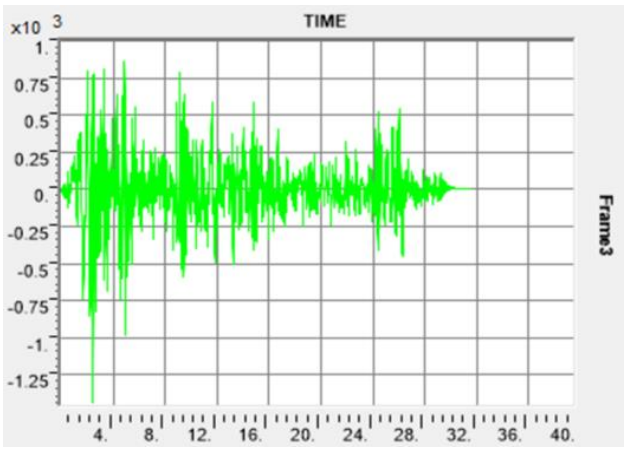

Figure 33.(3 3)bending moment of Element 3

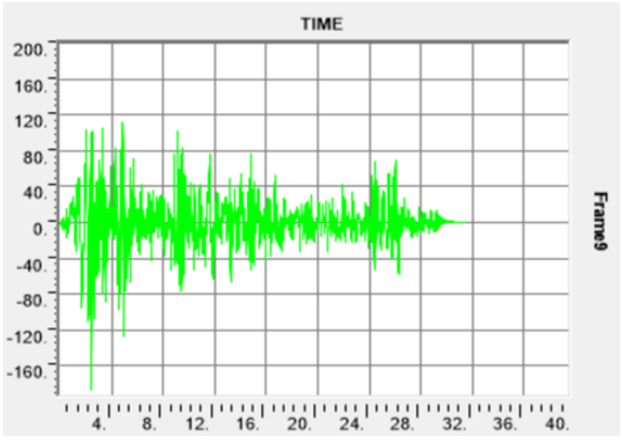

Figure 34. Axial force of Element 9

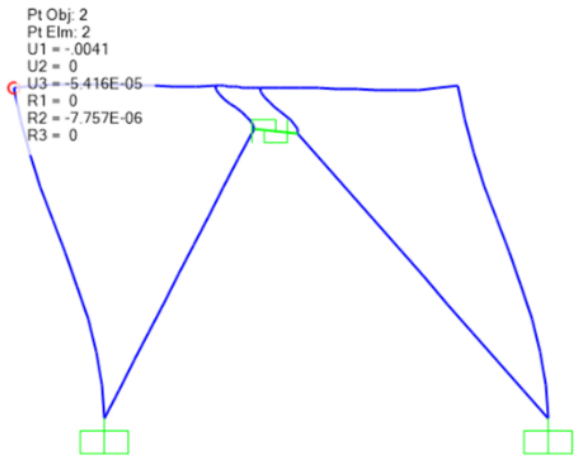

Figure 35. Envelope of frame displacement at Point 2

4.1.3. Examination of the results for the intermediate moment frame system with conventional concentric brace and damper

After analyzing and designing the intermediate moment frame and the conventional concentric brace with the damper, the El Centro earthquake spectrum was input into the software, the corresponding load cases were defined, and the outputs were extracted. Figure 25 shows the numbering of the points (nodes). Figures26and 27 show the PSA diagrams at Points 12 and 1 in the X direction, respectively. Figures 28 and 29 show the displacement of Points 2 and 13 under the earthquake. Figures 30 and 31 display the velocity variation of Points 1 and 13 under the El Centro earthquake. Figures 32 and 33 illustrate the 3-3 bending moment for Elements 1 and 3, respectively. Figure 34 shows the axial force of Element9. Finally, Figure 35 shows the envelope of frame displacementvalues atPoint 2.

4.2. Summary Comparison of the Performance of the Three Models

Table 3 presents the key seismic response values of the studied frame.

Table 3.
Summary of seismic response parameters for the three models

Parameter	Model M1	Model M2 (IMF+Chevron)	Model M3 (IMF+Chevron+RFD)
Maximum roof displacement (cm)	0.60	0.001	0.0041
Inter-story drift (%)	0.20	0.00033	0.00137
Maximum velocity (m/s)	0.05	0.002	0.007
Maximum beam bending moment (kN·m)	~3.5	~1.2	~1.0
Maximum brace axial force (kN)	–	~15	~12
First mode period (s)	0.3247	0.0790	~0.0785

4.3. Analysis and Interpretation of Results

From the numerical results presented in Table 3 and the observations from the time-history plots of displacement, bending moment, axial force, and velocity, the following analyses can be concluded:

4.3.1. Analysis of Displacements and Drift

The maximum roof displacement values in Table 3 show that the simple moment frame (M1), with a displacement of 0.60 cm, is the softest system. This displacement corresponds to a drift of 0.20%, which is within the code allowable limit (typically 1%) but indicates a lack of lateral stiffness. With the addition of the chevron brace (Model M2), the roof displacement is drastically reduced to 0.001 cm, which is a 99.83% reduction compared to M1. This reduction is mainly due to an extraordinary increase in lateral stiffness; the first mode period decreases from 0.3247 s to 0.0790 s (a 75.7% reduction). Such high stiffness makes the structure behave essentially as a rigid body, with its displacement falling within the measurement error range. The braces sustain axial forces up to 15 kN, and all earthquake energy is absorbed as elastic force in them.

Model M3, in which an RFD is added to the same braced frame, shows a roof displacement of 0.0041 cm (i.e., about four times that of Model M2). This slight increase in displacement – which at first glance might be seen as negative – is actually an indication of damper activation, allowing a controlled relative motion for energy dissipation. In fact, in M2 the braces are locked and permit no movement, whereas in M3 the damper, through its rotational slip, allows a very small displacement (less than 0.05 mm) to occur so that energy can be dissipated. This phenomenon is similar to the action of a fuse: the damper allows the main member (the brace) to remain in the elastic range and to sustain a lower force.

4.3.2. Analysis of Internal Forces

Beam bending moment: The maximum beam bending moment in Model M1 is about 3.5 kN·m. In Model M2, this value decreases to 1.2 kN·m (a 65.7% reduction), and in Model M3 it reaches 1.0 kN·m (a 71.4% reduction compared to M1). Importantly, there is a 16.7% reduction in moment in M3 compared to M2 (from 1.2 to 1.0 kN·m). This reduction in moment occurs despite the slight increase in displacement in M3 (from 0.001 to 0.0041 cm), indicating that the energy dissipation mechanism in the damper reduces the need for bending moment in the beam. In other words, part of the energy that was stored as beam moment in M2 is dissipated as friction in the RFD in M3.

Brace axial force: Comparing the brace axial force between M2 (15 kN) and M3 (12 kN) shows a 20% reduction. This is one of the most important findings of this study: adding the RFD, without significantly reducing stiffness, considerably reduces the force transmitted to the

braces. This feature is highly valuable in seismic design, because braces and their connections can be designed for a lower force while simultaneously increasing seismic safety.

4.3.3. Analysis of Velocity and Dynamic Stability

The velocity plots show that in Model M1, the velocity amplitude is relatively high (about 0.05 m/s) and velocity oscillations decay slowly (low damping). In Model M2, the velocity is very low (on the order of 0.002 m/s) and oscillations damp out quickly, but this damping is due to inherent structural damping, not a dissipative mechanism. In Model M3, the velocity amplitude is slightly higher than in M2 (about 0.005–0.01 m/s), but the rate at which oscillations decay is much faster. This behavior indicates that the equivalent damping provided by the RFD plays an effective role in reducing the settling time of the dynamic response. In practice, this means a reduction in the duration of structural vibration after the earthquake ends and a reduction in occupant discomfort.

4.3.4. Effect of Period and Frequency Content of the Earthquake

The El Centro earthquake has a rich frequency content in the range of 0.1 to 10 Hz. The first mode period of M1 (0.3247 s, equivalent to 3.08 Hz) lies within the effective excitation range of this earthquake. The periods of M2 and M3 (about 0.079 s, equivalent to 12.66 Hz) lie in the high frequency range of the earthquake, where the spectral acceleration is lower. Therefore, part of the response reduction in M2 and M3 is due to moving away from the resonance range. However, the reduction in brace axial force in M3 relative to M2 cannot be explained by the period change (the period of M3 is almost equal to that of M2) and is solely due to the equivalent damping of the damper.

5. Discussion

In this study, an equivalent linear model for the Rotational Friction Damper (RFD) based on the work energy equivalence principle was developed and implemented in ETABS software as a linear Link element with a rotational degree of freedom. The performance of this model was evaluated on a one story, one bay steel frame under the El Centro earthquake record and compared with two other common systems: an intermediate moment frame and a moment frame with a chevron brace. The main findings are as follows:

- Model M1 (moment frame) has the weakest seismic performance (largest displacement, largest moment, long lasting oscillations).
- Model M2 (chevron braced frame) drastically reduces displacement but transfers all earthquake energy as internal force to the braces. This system is excellent from the viewpoint of displacement control but is ineffective in reducing member forces.
- Model M3 (braced + RFD), by accepting a very slight increase in displacement (from 0.001 to 0.0041 cm – an increase that is negligible in practice), succeeds in reducing the brace axial force by 20% and the beam bending moment by 16.7% (compared to M2). This means an improvement in seismic performance without a noticeable reduction in stiffness.

Therefore, the Rotational Friction Damper not only does not increase displacement (the increase is so small that it is negligible in practice), but also, by dissipating energy, reduces the load on the primary structural members and improves dynamic stability. These characteristics make the RFD an attractive option for performance based seismic design, especially in structures where the goal is to maintain linear behavior of the primary members under design level earthquakes.

References

[1] Titirla, M.D. (2023). A State-of-the-Art Review of Passive Energy Dissipation Systems in Steel Braces. Buildings, *13*(4), 851. https://doi.org/10.3390/buildings13040851

[2] Soong, T.T., & Spencer, B.F. (2002). Supplemental Energy Dissipation: State-of-the-Art and State-of-the-Practice. Engineering Structures, *24*(3), 243-259. https://doi.org/10.1016/S0141-0296(01)00092-X

[3] Spencer, B.F., Jr., & Nagarajaiah, S. (2003). State of the art of Structural Control. Journal of Structural Engineering, *129*(7), 845-856. https://doi.org/10.1061/(asce)0733-9445(2003)129:7(845)

[4] Pall, A., & Pall, R. (2004). Performance Based Design Using Pall Friction Dampers – An Economical Design Solution. 13th World Conference on Earthquake Engineering.

[5] Tiwary, A., Tiwari, A., & Kumar, A. (2014). State-of-Art in Active, Semi-Active and Hybrid Control Systems for Tall Buildings. International Journal of Engineering Research and Applications, *4*(1), 1-5.

[6] DAMPTECH. (2023). Friction Dampers for Seismic Protection. Available online: www.damptech.com

[7] Pall, A.S., & Marsh, C. (1982). Seismic Response of Friction Damped Braced Frames. Journal of the Structural Division, *108*(6), 1313-1323. https://doi.org/10.1061/jsdeag.0005968

[8] Mualla, I.H., & Belev, B. (2002). Performance of Steel Frames with a New Friction Damper Device under Earthquake Excitation. Engineering Structures, *24*(3), 365-371. https://doi.org/10.1016/s0141-0296(01)00102-x

[9] Pall, A.S., Verganelakis, V., & Marsh, C. (1987). Friction-Dampers for Seismic Control of Concordia University Library Building. Proceedings of the 5th Canadian Conference on Earthquake Engineering, 191-200.

[10] Papadopoulos, P. (2012). New Nonlinear Anti-Seismic Steel Device for the Increasing the Seismic Capacity of Multi-Storey Reinforced Concrete Frames. The Structural Design of Tall and Special Buildings, *21*(10), 750-763. https://doi.org/10.1002/tal.648

[11] Javidan, M.M., & Kim, J. (2022). A Rotational Friction Damper-Brace for Seismic Design of Resilient Framed Structures. Journal of Building Engineering, *51*, 104248. https://doi.org/10.1016/j.jobe.2022.104248

[12] Mualla, I.H. (2015). Analysis, Design and Applications of Rotational Friction Dampers for Seismic Protection. Journal of Civil Engineering and Environmental Architecture, *62*(4), 335-346.

[13] Javidan, M.M., & Kim, J. (2019). Seismic Retrofit of Soft-First-Story Structures Using Rotational Friction Dampers. Journal of Structural Engineering, *145*(12), 04019162. https://doi.org/10.1061/(ASCE)ST.1943-541X.0002433

[14] Sano, T., Shirai, K., Suzui, Y., & Utsumi, Y. (2019). Loading Tests of a Brace-Type Multi-Unit Friction Damper using Coned Disc Springs and Numerical Assessment of its Seismic Response Control Effects. Bulletin of Earthquake Engineering, *17*, 5365-5391.

[15] Veismoradi, S., Yousef-beik, S.M.M., Zarnani, P., & Quenneville, P. (2021). Development and Parametric Study of a New Self-Centering Rotational Friction Damper. Engineering Structures, *235*, 112097. https://doi.org/10.1016/j.engstruct.2021.112097

[16] Oliaei, M., Mashhadiyan, M., & Forootan, R. (2023). Seismic Performance Evaluation of Friction Damper and Yielding Metallic Damper in Steel Frame. Journal of Civil Engineering Researchers, *5*(3), 1–14. https://doi.org/10.61186/JCER.5.3.1

[17] Mahdizade, A., & Rakhshandeh Abadi, M. (2017). Structural Analysis and Design of a 30‐Story Tower with Friction Dampers. Journal of Civil Engineering Researchers, *7*(4), 68–77.

[18] Tahara, S., Iwaya, K., Iwashita, T., Goto, K., & Yamanari, M. (2024). Strength Estimation and Fundamental Characteristics of the New Rotational Friction Damper with Translational Movement. Machines, *12*(1), 15. https://doi.org/10.3390/machines12010015

[19] Filiatrault, A., & Cherry, S. (1990). Seismic Design Spectra for Friction-Damped Structures. Journal of Structural Engineering, *116*(5), 1334-1355. https://doi.org/10.1061/(asce)0733-9445(1990)116:5(1334)

[20] Sui, W., Wang, X., & Wang, Z. (2021). Experimental Study on Mechanical Properties of the Steel Friction Pads used in a Rotational Friction Damper. Structures, *29*, 1808-1818. https://doi.org/10.1016/j.istruc.2020.11.079